the FEBS Journal

The ROQUIN family of proteins localizes to stress granules via the ROQ domain and binds target mRNAs

Vicki Athanasopoulos[1,2,*], Andrew Barker[3,*], Di Yu[4], Andy H-M. Tan[1], Monika Srivastava[1], Nelida Contreras[2], Jianbin Wang[2], Kong-Peng Lam[5], Simon H. J. Brown[6], Christopher C. Goodnow[1], Nicholas E. Dixon[6], Peter J. Leedman[3,7], Robert Saint[2,8] and Carola G. Vinuesa[1]

1 The John Curtin School of Medical Research, The Australian National University, Canberra, Australia
2 ARC Special Research Centre for the Molecular Genetics of Development (CMGD), Research School of Biology, Canberra, Australia
3 Laboratory for Cancer Medicine, The University of Western Australia Centre for Medical Research, Western Australian Institute for Medical Research, Perth, Australia
4 Immunology and Inflammation Research Program, Garvan Institute of Medical Research, Sydney, Australia
5 Laboratory of Immunology, Bioprocessing Technology Institute, Agency for Science, Technology and Research (A*STAR), Singapore
6 School of Chemistry, University of Wollongong, Australia
7 School of Medicine and Pharmacology, The University of Western Australia, Crawley, Australia
8 Department of Genetics, University of Melbourne, Australia

Keywords
membrane-associated nucleic acid binding protein; microRNA; ROQ; ROQUIN; stress granules

Correspondence
C.G. Vinuesa, The John Curtin School of Medical Research, The Australian National University, Garran Road, PO Box 34, ACT 2601, Australia
Fax: +61 2 6125 2595
Tel: +61 2 6125 4500
E-mail: carola.vinuesa@anu.edu.au

*These authors contributed equally to this article

(Received 22 December 2009, revised 18 February 2010, accepted 25 February 2010)

doi:10.1111/j.1742-4658.2010.07628.x

Roquin is an E3 ubiquitin ligase with a poorly understood but essential role in preventing T-cell-mediated autoimmune disease and in microRNA-mediated repression of inducible costimulator (*Icos*) mRNA. Roquin and its mammalian paralogue membrane-associated nucleic acid binding protein (MNAB) define a protein family distinguished by an ~200 amino acid domain of unknown function, ROQ, that is highly conserved from mammals to invertebrates and is flanked by a RING-1 zinc finger and a CCCH zinc finger. Here we show that human, *Drosophila* and *Caenorhabditis elegans* Roquin and human MNAB localize to the cytoplasm and upon stress are concentrated in stress granules, where stalled mRNA translation complexes are stored. The ROQ domain is necessary and sufficient for localization to arsenite-induced stress granules and to induce these structures upon overexpression, and is required to trigger *Icos* mRNA decay. Gel-shift, SPR and footprinting studies show that an N-terminal fragment centred on the ROQ domain binds RNA from the *Icos* 3′-untranslated region comprising the minimal sequence for Roquin-mediated repression, adjacent to the miR-101 sequence complementarity. These findings identify Roquin as an RNA-binding protein and establish a specific function for the ROQ protein domain in mRNA homeostasis.

Structured digital abstract

- MINT-7711163: *TIA-1* (uniprotkb:P31483) and *Roquin* (uniprotkb:Q4VGL6) *colocalize* (MI:0403) by *fluorescence microscopy* (MI:0416)
- MINT-7711475: *RLE-1* (uniprotkb:O45962) and *TIA-1* (uniprotkb:P31483) *colocalize* (MI:0403) by *fluorescence microscopy* (MI:0416)
- MINT-7711487: *DmRoquin* (uniprotkb:Q9VV48) and *TIA-1* (uniprotkb:P31483) *colocalize* (MI:0403) by *fluorescence microscopy* (MI:0416)

Abbreviations

Dcp1a, decapping enzyme 1; FMRP, Fragile X mental retardation protein; G3BP, Ras-GAP SH3 domain-binding protein; GFP, green fluorescent protein; *Icos*, inducible costimulator; miRNA, microRNA; MNAB, membrane-associated nucleic acid binding protein; REMSA, RNA electrophoresis mobility shift assay; TIA, T-cell intracellular antigen; TIS11, TPA-induced sequence 11; TTP, tristetraprolin.

- MINT-7711447, MINT-7711460: *MNAB* (uniprotkb:Q9HBD1) and *TIA-1* (uniprotkb:P31483) *colocalize* (MI:0403) by *fluorescence microscopy* (MI:0416)
- MINT-7711176: *eIF3* (uniprotkb:P55884) and *Roquin* (uniprotkb:Q4VGL6) *colocalize* (MI:0403) by *fluorescence microscopy* (MI:0416)
- MINT-7711192: *DCP1A* (uniprotkb:Q9NPI6) and *TIA-1* (uniprotkb:P31483) *colocalize* (MI:0403) by *fluorescence microscopy* (MI:0416)

Introduction

Roquin, encoded by the *Rc3h1* gene, was recently identified as a novel RING-type ubiquitin ligase family member. *Sanroque* mice, homozygous for the *Rc3h1* '*san*' missense allele (M199R), develop a lupus-like pathology. Roquin$^{san/san}$ mice express higher levels of the T-lymphocyte costimulatory receptor ICOS in a T-cell-autonomous fashion, and have increased numbers of germinal centres and follicular helper T cells. We have recently shown that failure of Roquin to repress *Icos* mRNA through the microRNA (miRNA) machinery in T cells contributes to autoimmune lymphoproliferation in *sanroque* mice [1]. The protein contains an extraordinarily conserved and novel domain, termed the ROQ domain, located in the N-terminus of the protein [2]. To date, it is not known how Roquin localizes to stress granules and regulates its mRNA targets or what the function of the unique ROQ domain is in this process.

Recent findings have illuminated an important but poorly understood set of cytoplasmic structures and proteins involved in the action of miRNAs and the control of mRNA stability. Stress granules are cytoplasmic aggregates that form when eukaryotic cells are subjected to a range of environmental stresses such as oxidative conditions, heat, UV irradiation and some viral infections [3]. Stress granules are thought to aid recovery from potentially lethal stresses by disrupting general mRNA translation, permitting preferential expression of stress proteins (heat shock proteins) that repair intracellular damage and restore cellular homeostasis [4]. Consistent with this, most known components of stress granules, including T-cell intracellular antigen (TIA)-1/TIA related [5], tristetraprolin (TTP), Ras-GAP SH3 domain-binding protein (G3BP) [6], PABP-I, HuR [7], eIF3, eIF4, eIF4G and Fragile X mental retardation protein (FMRP) [8], are involved in regulating mRNA transport, translation, stability or degradation [9]. Regulation of mRNA metabolism has also been shown to be important for attenuating translation of inflammatory mediators. For example, TRAF2 is sequestered in stress granules during stress, where it interacts with the translation initiation factor scaffold protein eIF4GI and inhibits tumour necrosis factor signalling and activation of NF-κB [10]. Similarly, naive T-helper cells have been shown to undergo a stress-type response (termed the integrated stress response) after receiving an initial priming signal through the T-cell receptor [11].

Stress granules have been shown to be spatially, compositionally and functionally linked to GW bodies/processing or P-bodies, which are distinct cytoplasmic sites at which mRNAs undergo general 5′–3′, nonsense-mediated or miRNA/RNAi-mediated degradation [9,12–16] but where mRNAs may also be transiently stored and rerouted to polysomes to be translated [17]. P-bodies are highly mobile within the cytoplasm, intermittently attaching to stress granules [14]. Factors such as the cytoplasmic polyadenylation element-binding protein [18] and the mRNA-destabilizing protein TTP with its related protein BRF1, promote interactions between stress granules and P-bodies [14]. In view of these interactions, stress granules have been proposed as sites of triage to which untranslated transcripts are shuttled in response to stress and where their subsequent fate, release to complete translation or transfer to P-bodies for further storage or degradation, is decided [19].

Here we show that endogenous Roquin localizes to the nucleus and cytoplasm and, upon environmental stress, concentrates in stress granules. The novel ROQ domain mediates localization to stress granules and induces spontaneous stress granule formation upon overexpression; a function that is shared by the analogous region from the mammalian paralogue, membrane-associated nucleic acid binding protein (MNAB), and the worm and fly orthologues, RLE-1 and DmRoquin, respectively. Furthermore, we show that Roquin binds directly to *Icos* mRNA and that the ROQ domain is required for repression of *Icos* mRNA by Roquin in T cells.

Results

Roquin family members localize to stress granules and induce their formation

We previously observed that mouse Roquin protein fused to green fluorescent protein (GFP) localizes to

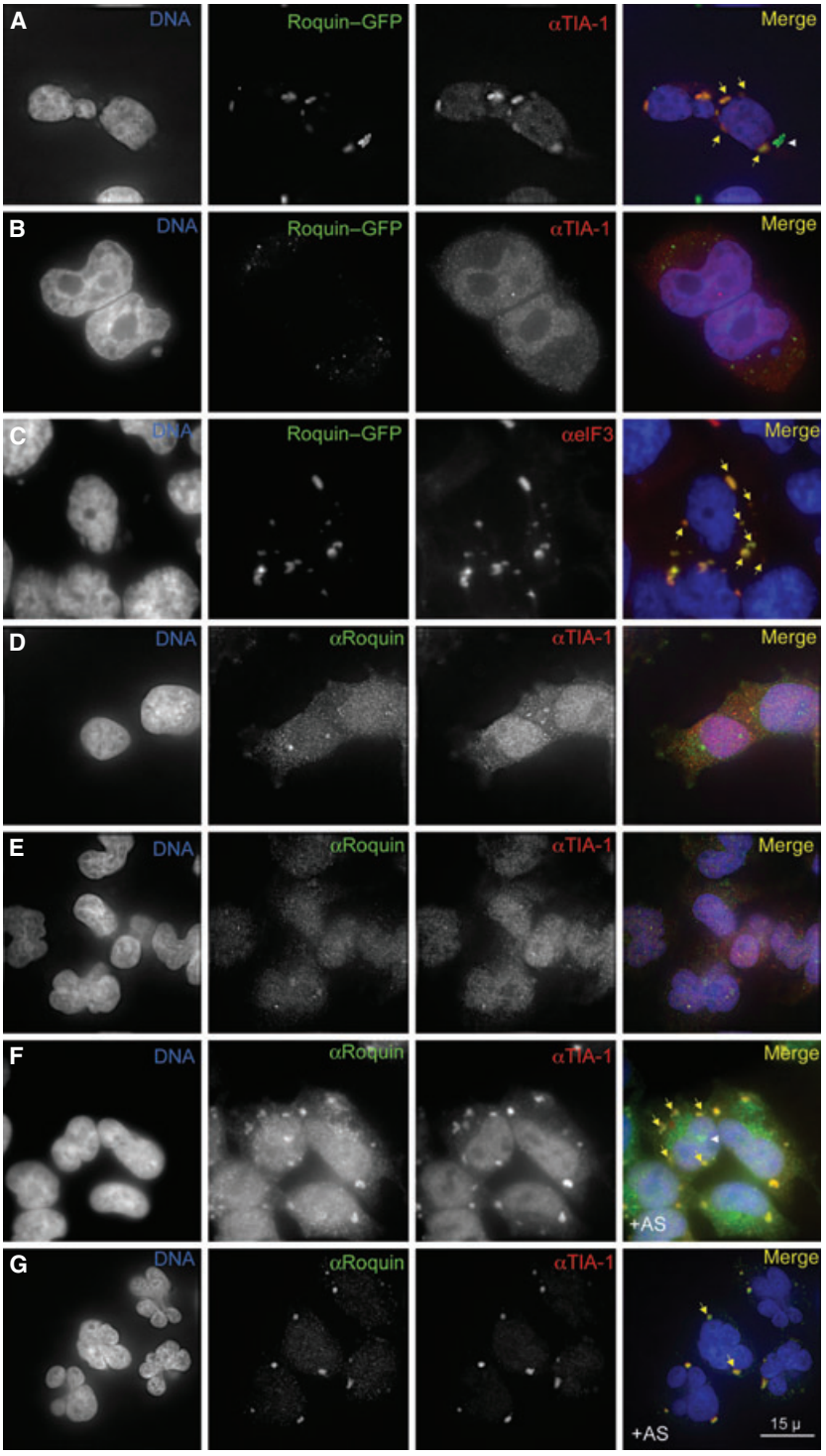

Fig. 1. Roquin is recruited to stress granules (SGs). (A–C) HEK 293T cells were transfected with Roquin–GFP (shown in green), fixed and stained with anti-TIA-1 (red in A,B) or anti-eIF3 IgG (red in C). Ectopically expressed Roquin–GFP localizes to either TIA-1 (yellow arrows in A) or eIF3 (yellow arrows in C) positive stress granules or to fine puncta which do not costain with TIA-1 (B). In A, white arrowheads show Roquin granules lacking TIA-1. HEK 293T cells (D) and Jurkat cells (E) were double-stained with anti-Hs Roquin (green) and anti-TIA-1 (red) IgG to allow detection of the endogenous proteins, which localize diffusely throughout the cytoplasm and nucleus. HEK 293T cells (F) and Jurkat cells (G) were treated with sodium arsenite (+AS) for 1 h to induce stress granule formation, then double-stained with anti-Roquin (green) and anti-TIA-1 IgG (red). Yellow arrows in (F) and (G) indicate Roquin granules within one particular cell which are positive for TIA-1. White arrowhead in (F) indicates Roquin granule lacking TIA-1. DNA is stained with 4′,6-diamidino-2-phenylindole (blue).

TIA-1-positive cytoplasmic granules when expressed in arsenite-stressed HEK 293T cells [2], suggesting that Roquin localizes to stress granules. During the course of our experiments, we observed that a large fraction of nonarsenite-treated cells (~ 30% of transfected cells) formed granules that contained endogenous TIA-1 (Fig. 1A). Because these cells had not been chemically stressed, it appeared that Roquin overexpression was inducing stress granules (Fig. 1A, yellow arrows). In some cells, generally those lacking obvious

TIA-1$^+$ granules, Roquin appeared to be localized diffusely in small puncta throughout the cytoplasm (Fig. 1B). Careful analysis indicated that a small proportion ($\sim 2\%$) of Roquin granules within cells containing TIA-1$^+$ granules did not colocalize with TIA-1 (Fig. 1A, white arrowhead). Because TIA-1 is not a universal marker of stress granules (i.e. does not localize to all G3BP-induced stress granules) [6], it is possible that these TIA-1-negative Roquin granules are bona fide stress granules. Costaining with an antibody that detects endogenous eIF3, a component of the translational machinery that is uniquely present in stress granules revealed that Roquin granules contained eIF3 (Fig. 1C). Cycloheximide treatment, which normally causes disassembly of stress granules, resulted in the slow dispersal of most ectopically expressed Roquin and/or TIA-1$^+$ granules, indicating that these do not consist of cleaved recombinant proteins in aggresomes [20], but are bona fide stress granules (Fig. S1A,B). Furthermore, overexpression of GFP250, a cytosolic protein chimera that typically causes the formation of aggresomes [21], induced typical aggresomes in 293 T cells that were not positive for either TIA-1 or for endogenous Roquin (Fig. S1C).

To confirm that localization was not an artefact caused by ectopic expression of Roquin–GFP or the presence of a tag on the C-terminus of the protein, we analysed the localization of endogenous Roquin by performing immunofluorescence using a specific antibody against Roquin (Fig. S1D,E) in HEK 293T cells (Fig. 1D) and the human T-cell line Jurkat (Fig. 1E). Roquin showed a diffuse distribution throughout the cytoplasm and nucleus in both cell types (Fig. 1D,E), as well as in HeLa and NIH3T3 cells (Fig. S1E). Although it is possible that the nuclear staining was nonspecific, there were no visible nonspecific bands on western blots performed using the same antibody on HEK 293 T cell lysates (data not shown). These results show that Roquin is expressed in a range of cell lines, consistent with the widespread mRNA expression data [2]. Upon treatment with sodium arsenite to induce oxidative stress, the protein localized to discrete puncta that were also positive for TIA-1 (Fig. 1F,G). These data indicate that both endogenous and ectopically expressed Roquin are recruited to stress granules.

Roquin does not localize to P-bodies or endosomal compartments

Stress granules and P-bodies have been shown to share several RNA-binding proteins (e.g. TTP, Fas-activated serine/threonine phosphoprotein, XRN1 and eIF4E), although other RNA-binding proteins are found only in stress granules (eIF3, G3BP, eIF4G and PABP-1) or P-bodies (decapping enzyme [DCP]1a and 2 and GW182) [9,14]. Roquin contains a putative RNA-binding domain of the rare Cx8Cx5Cx3H type also found in TTP, which shuttles from stress granules to P-bodies and regulates the stability of short-lived transcripts, including the proinflammatory cytokine tumour necrosis factor. The presence of this domain and our recent observation that *Icos* mRNA localizes to both stress granules and P-bodies [1] suggested that Roquin may also regulate mRNA metabolism within P-bodies. To visualize P-bodies, HEK 293T cells were cotransfected with either human Dcp1a–GFP and/or Dcp1a–DsRed; both of which displayed identical localization to typical TIA-1$^-$ P-bodies (Fig. 2A,B). Cotransfection of Dcp1a–DsRed and Roquin–GFP revealed that although the two proteins were often in very close proximity they did not appear to colocalize, suggesting that Roquin is not a component of P-bodies (Fig. 2C). Similar results were obtained after arsenite-treated HEK 293T cells transfected with Dcp1–GFP (Fig. 2D,E) were stained for endogenous Roquin (Fig. 2E), and in cells transfected with Roquin–GFP and stained for endogenous DCP-1 (data not shown).

Roquin contains a RING-1 finger domain that is shared by many E3 ubiquitin ligases, and the worm orthologue, RLE-1, has been shown to possess ubiquitin ligase activity [22]. A large number of E3 ubiquitin ligases, including Cbl [23], Nedd4, Itch (reviewed in [24,25]), POSH [26] and Pib1p [27], are involved in endocytic protein sorting and localize to endosomal compartments. To test whether Roquin may also localize to a cytosolic compartment different from stress granules we used Hrs protein fused to GFP or DsRed as a marker of early endosomes, but observed no colocalization with Roquin–GFP in HEK 293T cells (Fig. 2F,G). Similarly, endogenous Roquin did not colocalize with Hrs in cells expressing GFP–Hrs and displaying the reported fine punctate staining pattern (Fig. 2H). Because Roquin mRNA is expressed in a diverse range of tissues and cell types [2], we cannot rule out the possibility that the protein may localize differently in other cells because of interactions with different partners.

Roquin orthologues and paralogue, MNAB, also localize to stress granules

The single Roquin-like paralogue in humans and mice, MNAB, possesses a similar domain architecture to Roquin and shows a high degree of sequence conservation (65% identity and 75% similarity) in the N-terminus, which includes the RING-1/E3 ligase zinc finger,

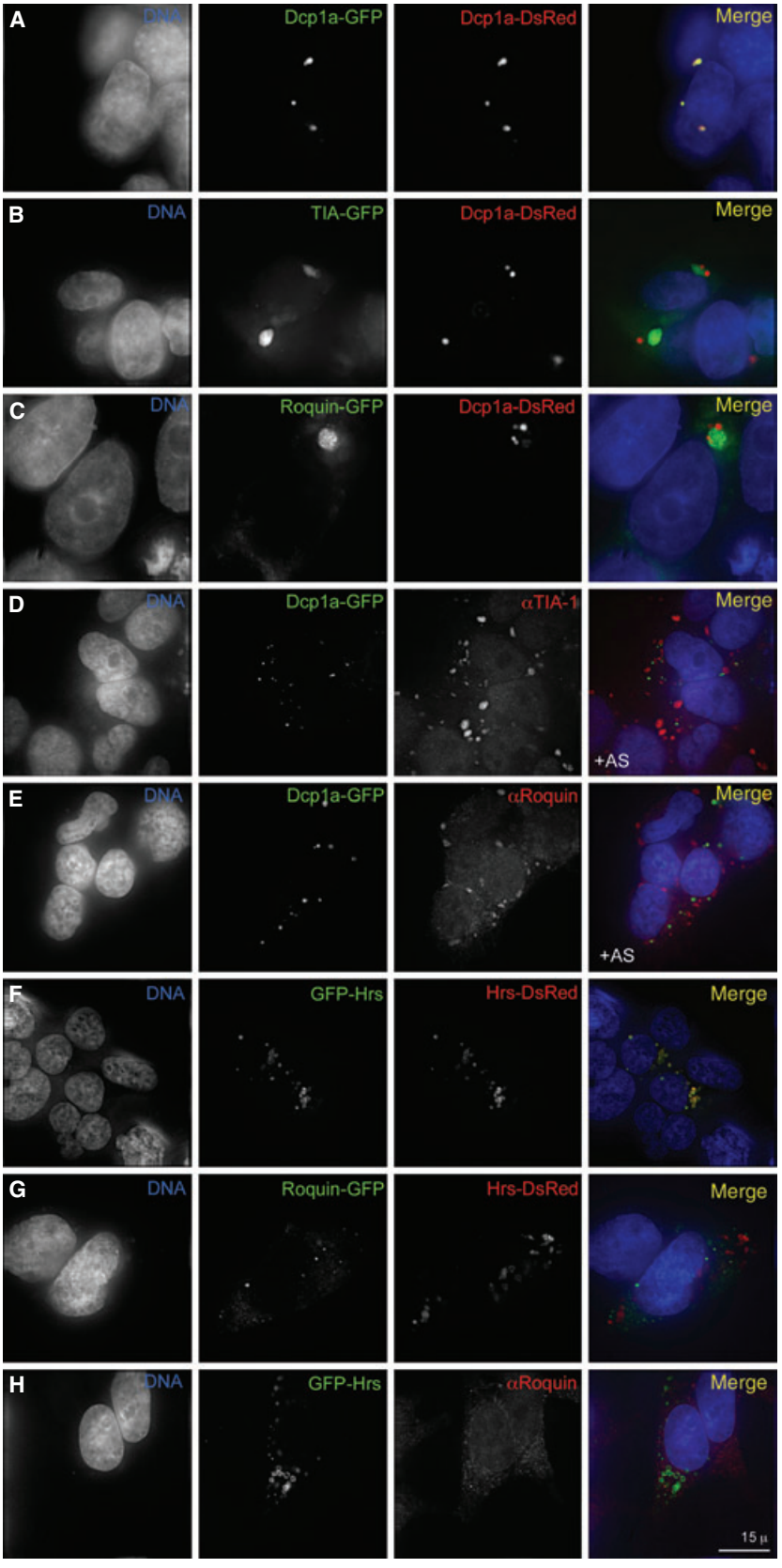

Fig. 2. Roquin does not localize to P-bodies or to early endosomes. (A) HEK 293T cells were cotransfected with Hs Dcp1a–GFP (green) and Dcp1a–DsRed (red) as a colocalization control or (B) with GFP-tagged Hs TIA-1 (green) and Dcp1a–DsRed (red), and (C) with Roquin–GFP (green) and Dcp1a–DsRed (red). After 48 h, cells were fixed and counterstained with 4′,6-diamidino-2-phenylindole (blue). (D–E) HEK 293T cells were transfected with Dcp1a–GFP (green) and stained with either the anti-TIA-1 IgG (red in D) or for endogenous Roquin (αRoquin, red in E) after stress induction with 1 mM sodium arsenite (+AS). (F,G) HEK 293T cells were cotransfected with GFP–Hrs (green) and Hrs–DsRed as a colocalization control (red) (F) or Roquin–GFP (green) and Hrs–DsRed (red) (G), then fixed and counterstained with 4′,6-diamidino-2-phenylindole (blue). (H) HEK 293T cells were transfected with GFP–Hrs (green) and stained with anti-Roquin IgG (red).

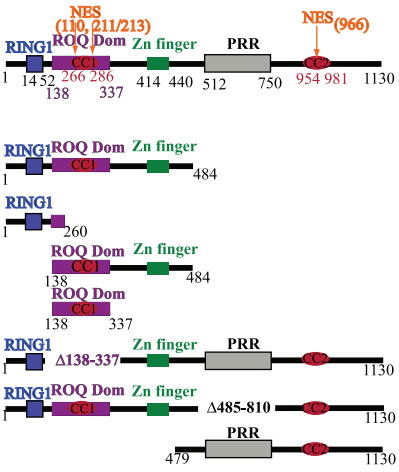

	SG induction (%)	SG recruitment (%)
GFP	10	2
1–1130	32	96
1–1130 + M199R	33	99
1–1130 + C434R	38	100
1–484	24	98
1–484 + C434R	18	100
1–260	23	0
138–484	33	93
138–337	25	93
1–1130 + Δ138–337	12	0
1–1130 + Δ485–810	24	100
479–1130	24	11

Fig. 3. Schematic representation of the various proteins transfected into HEK 293-T cells and their ability to induce spontaneous TIA-1-positive stress granules (stress granule induction), and to colocalize with TIA-1 granules (stress granule recruitment). Results are the average of at least two experiments with counts of over 120 cells per experiment.

ROQ, coiled-coil (CC1) and CCCH zinc-finger domains, but diverges in the C-terminal domains. Furthermore, MNAB and the *Caenorhabditis elegans* and *Drosophila melanogaster* Roquin orthologues, RLE-1 and DmRoquin, respectively, also show high conservation in the first 450 amino acids, (~ 75% similarity). We therefore investigated whether these three Roquin family members also localize to stress granules when ectopically expressed in HEK 293T cells.

Like Roquin, human MNAB–GFP shows either larger stress granule-like structures, which are positive for TIA-1 staining (Fig. S2A) or a fine punctate distribution which does not colocalize with TIA-1 when overexpressed in 293 T cells (not shown). The endogenous MNAB protein was also recruited to TIA-1$^+$ stress granules under conditions of oxidative stress (Fig. S2E). When co-expressed, Roquin and MNAB colocalize at stress granule-like structures (data not shown). Ectopic expression of RLE-1 (Fig. S2B) and DmRoquin (Fig. S2C) in 293 T cells also induced the formation of granules that contained TIA-1. MNAB did not localize to GFP–Hrs endosomes when overexpressed in HEK 293T cells (Fig. S2D), which is at odds with the report of partial colocalization of endogenous MNAB in the A549 cell line (as well as COS7 and HeLa cells) with the transferrin receptor [28]. MNAB has been reported to also localize to cell membranes and this has been proposed to be because of the hydrophobic C-terminus of the protein, a region absent in the shorter Roquin protein [28]. Although we could not detect membrane localization of the ectopically expressed tagged MNAB proteins, there was nonuniform membrane localization of endogenous MNAB between adjoining cells (Fig. S2E).

The novel and highly conserved ROQ domain mediates induction and recruitment to stress granules

HsROQUIN, HsMNAB, RLE-1 and DmRoquin are highly conserved in the N-terminus and all localize to stress granules, suggesting that this region may play a role in the localization and/or induction of stress granules. To determine the domain(s) responsible for induction and/or recruitment of Roquin to stress granules, we took advantage of the observation that ectopic expression of Roquin in HEK 293T cells induces stress granule formation and created a series of truncated Roquin proteins, as well as mutants lacking various domains (Fig. 3). All of these Roquin variants were fused to GFP and introduced into HEK 293T cells. The ability of each Roquin construct to spontaneously induce stress granules in transfected cells (in the absence of sodium arsenite) and to be recruited to stress granules (in an environment where all cells are forming stress granuless because of treatment with arsenite) was determined by staining cells for TIA-1 (Fig. S3A–I).

To ascertain the effect of the transfection process itself on stress granule induction, cells were transfected with GFP alone, and this resulted in a 10% induction of spontaneous stress granules with virtually no colocalization of TIA-1 and GFP (Fig. 3). Full-length Roquin (amino acids 1–1130) induced spontaneous stress granules in ~ 30% of transfected cells, and the

addition of sodium arsenite increased stress granule induction to 96% (Fig. 3). These results are comparable with another known stress granule inducer, FMRP [8]. A fragment spanning the highly conserved N-terminus of Roquin containing the RING-1, ROQ and CCCH domains (amino acids 1–484) induced comparable stress granule localization (Figs 3 and S3C). Similarly, the equivalent truncated form of MNAB containing the same three domains (amino acids 1–443) fused to GFP showed diffuse cytoplasmic staining dotted with TIA-positive stress granules confirming that the N-terminal regions of the Roquin-like homologues are indeed involved in stress granule formation/localization (Fig. S3F).

Previous work has indicated a link between the ubiquitin–proteasome pathway and the degradation of AU-rich transcripts [29]. To investigate whether the ubiquitin ligase domain (RING-1 Zn finger) of Roquin plays a role in its localization to stress granules, we introduced a C14A substitution predicted to disrupt the zinc-binding ability and E3 ligase activity [30], but saw no obvious effect on the recruitment of Roquin to stress granules (data not shown). To determine the role of the CCCH zinc-finger domain in protein localization, we introduced a mutation in the last cysteine (C434R), an alteration that has been shown to abolish the RNA-binding activity of TTP [31]. Both the full-length (1-1130 + C434R) and an N-terminal fragment of Roquin (1–484 + C434R) carrying the C434R substitution displayed stress granule localization (Figs 3 and S3A, and data not shown). These observations, together with the finding that a fragment consisting of the CCCH domain alone (amino acids 407–484) was ineffective in inducing or localizing to stress granules (Fig. S3E), suggest that the putative RNA-binding motif does not play a role in stress granule localization. Of note, the RLE-1 protein, which lacks a CCCH motif, is also able to localize to stress granules (Fig. S2B). We also investigated the effect of the M199R mutation, a nonconservative substitution within the highly conserved ROQ domain responsible for the lupus-like disease in *sanroque* mice [2], on stress granule induction and recruitment. Localization of wild-type Roquin and Roquin^{M199R} was found to be comparable (Figs 3 and S3B). In summary, these results show that localization to stress granules is determined by an N-terminal region distinct from the RING-1 or CCCH zinc fingers.

We next set out to delineate the minimal fragment within the N-terminal region involved in stress granule formation using nested truncations. A Roquin construct spanning amino acids 1–260 containing the E3-ligase RING finger alone showed a slight reduction in the ability to induce stress granules and importantly was not recruited to TIA-positive stress granules even in stressed cells (Figs 3 and S3D). By contrast, an extended fragment containing the RING finger and ROQ domains (amino acids 1–337; Fig. 4A), a fragment containing the ROQ domain and CCCH finger (amino acids 138–484; Fig. 4B) and a fragment containing exclusively the ROQ domain (amino acids 138–337; Fig. 4C) all localized to stress granules, suggesting that the ROQ domain is responsible for stress granule induction and localization. Two fragments spanning the N-terminal (amino acids 138-260; Fig. 4D) and C-terminal (amino acids 238–337; Fig. 4E) halves of the ROQ domain fused to GFP showed granular cytoplasmic distribution with no recruitment to TIA-1-positive stress granules, indicating that the entire domain is required for stress granule localization. Finally, to confirm that the ROQ domain is the minimal and essential region that determines localization to stress granules, we ectopically expressed a form of Roquin that exclusively lacked the ROQ domain (1–1130 + Δ138–337, Roquin$^{\Delta ROQ}$) and found minimal induction and localization to stress granules (Figs 3 and 4F).

To confirm that the C-terminus of the protein did not play an accessory role in stress granule induction or localization we deleted the whole proline-rich region, termed 1–1130Δ485–810 (Fig. 3), as well as looking at the localization of the proline-rich region alone (amino acids 498–817) and the C-terminal amino acids 818–1130. As expected from our N-terminal fusion data, deletion of the proline-rich region (1–1130Δ485–810) did not affect recruitment to stress granules (Fig. 3), and the proline-rich region and C-terminus did not localize to stress granules (Fig. S3G,H) confirming that the N-terminal domain of Roquin contains all the stress granule localization sequences.

The ROQ domain is required for Roquin's repression of *Icos* mRNA

We have recently found that Roquin prevents certain autoimmune manifestations through the repressive action of a particular microRNA (miR-101) on *Icos* mRNA stability [1]. ICOS expression is barely repressed by Roquin bearing the M199R mutation, which resides within the ROQ domain. To test whether the ROQ domain is involved in regulation of *Icos* expression, we used the pR-IRES–GFP retroviral vector [1], to express either Roquin^{WT}, Roquin^{M199R} or the Roquin construct lacking the ROQ domain – Roquin$^{\Delta ROQ}$ – ectopically in *roquin*$^{san/san}$ CD4$^+$ T cells. Although Roquin^{WT} reduces endogenous ICOS protein expression by

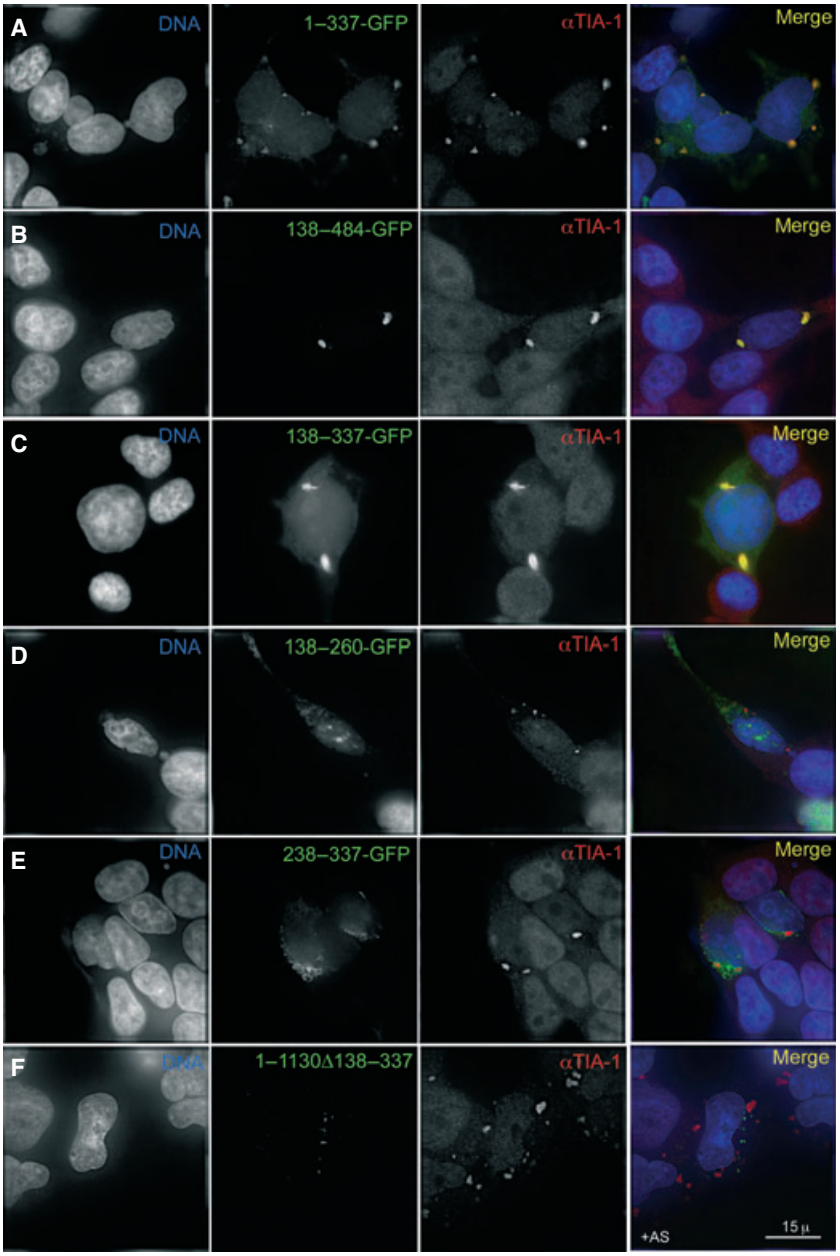

Fig. 4. The ROQ domain is the minimal region required for stress granule localization. HEK 293T cells were transfected with GFP-tagged Roquin fragments (green) spanning amino acids 1–337 (A), 138–484 (B), 138–337 (C), 138–260 (D), 238–337 (E) and a full-length fragment deleted for the ROQ domain (amino acids 1–1130Δ138–337 in F). After 48 h, cells were fixed and stained with anti-TIA-1 IgG (red). DNA is stained blue. Only fragments containing a complete ROQ domain are able to induce and localize to TIA-1-positive granules (A–C), whereas deletion (F) or disruption of the whole ROQ domain (D,E) abolish stress granule localization.

$\sim 50\%$, Roquin$^{\Delta ROQ}$ did not exert any measurable effect on *Icos* expression (Fig. 5A). This contrasts to the milder reduction in *Icos* expression ($\sim 20\%$) seen with Roquin^{M199R}, which unlike Roquin$^{\Delta ROQ}$ (Fig. 4F), can still localize to stress granules.

Roquin represses *Icos* mRNA expression by acting on its 3′-untranslated region (3′-UTR): when Roquin is expressed in NIH3T3 cells using the pR-IRES–GFP retroviral vector together with a pR-IRES–huCD4 retroviral vector expressing either full-length human *ICOS* cDNA (*huICOS*^{FL}) or *huICOS* cDNA lacking the 3′UTR (*huICOS*$^{\Delta 3'UTR}$), repression is only observed when *huICOS* is expressed from *huICOS*^{FL} [1]. This is a sensitive system with which to analyse Roquin's dose-dependent effects because GFP fluorescence can be used to infer relative Roquin levels in individual cells. NIH3T3 cells expressing high levels of Roquin consistently repress huICOS expression by $\sim 80\%$ [1] (Fig. 5B). When NIH3T3 cells were cotransduced with either Roquin^{WT}–IRES–GFP or Roquin$^{\Delta ROQ}$–IRES–GFP together with huICOS^{FL}–IRES–huCD4 or huICOS$^{\Delta 3'UTR}$–IRES–huCD4, we observed that Roquin$^{\Delta ROQ}$ was incapable of repressing huICOS expression (Fig. 5B). This also contrasts to

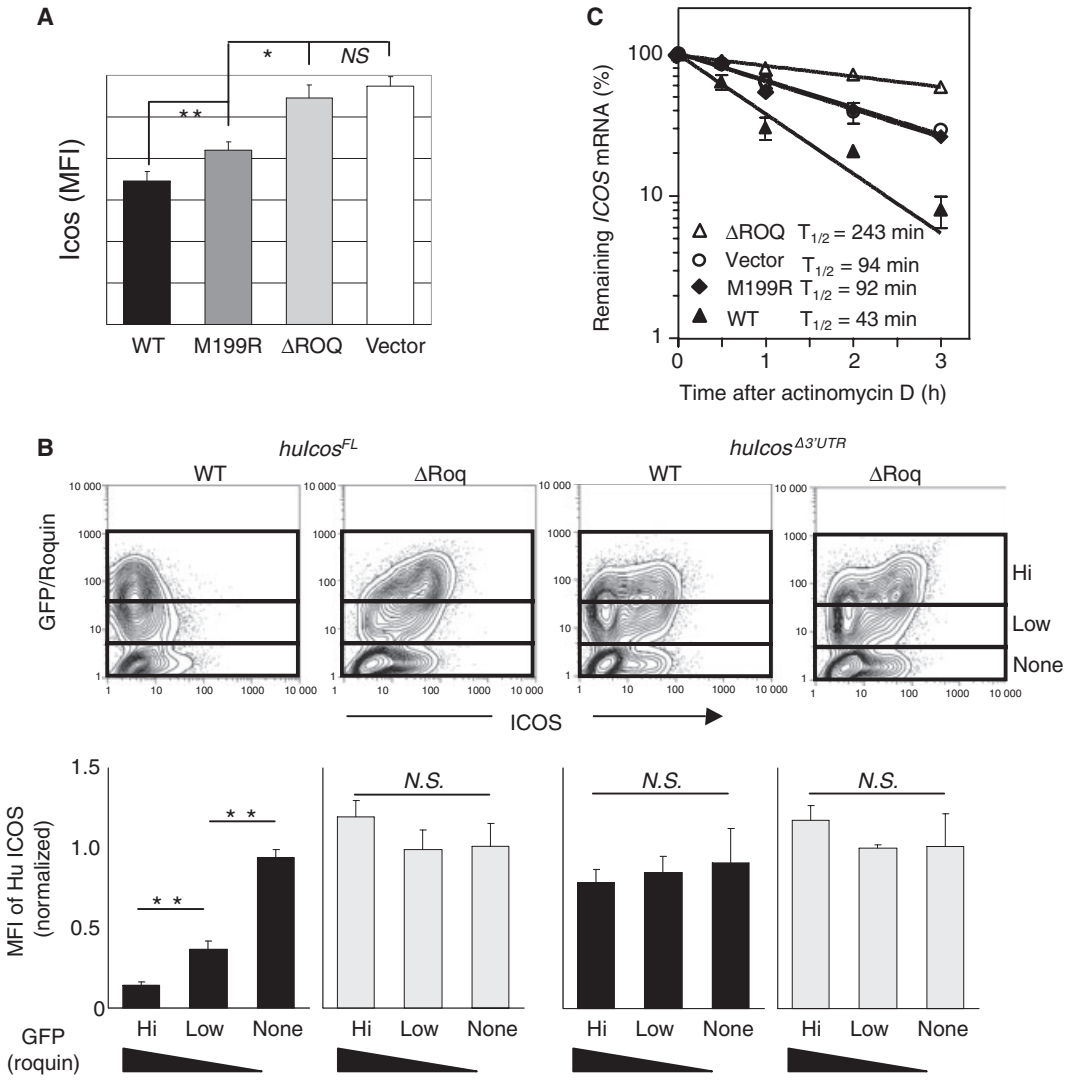

Fig. 5. The ROQ domain is required for Roquin's repression of *Icos* mRNA. (A) Mean fluorescent intensity (MFI) of ICOS on GFP$^+$ *Roquin*$^{san/san}$ CD4$^+$ T cells transduced with the indicated retrovirus. CD4$^+$ T cells magnetically isolated from *Roquin*$^{san/san}$ mice were stimulated with plate-bound anti-CD3ε (2 μg·mL^{-1}) plus anti-CD28 (5 μg·mL^{-1}) for 24 h before transduction with retroviruses as indicated. Cells were analysed by flow cytometry 4 days after retroviral transduction. (B) Upper: Flow cytometric contour-plots showing GFP and huICOS expression on NIH3T3 cells transduced with indicated *huICOS* vectors plus either Roquin^{WT} or Roquin$^{\Delta ROQ}$ vector. The boxes show the gates used to define the GFP^{Hi}, GFP^{Low} and GFP^{Nil} populations. Lower: MFI of huICOS in the populations gated in the upper panel. (C) *Icos* mRNA levels in activated EL4 cells transfected with Roquin^{WT}, Roquin ^{M199R} or Roquin$^{\Delta ROQ}$ vector or empty vector, treated with actinomycin D for the times indicated. Endogenous *Icos* mRNA levels were measured using real-time RT-PCR and normalized to β-actin. The amount of *Icos* mRNA at time 0 h was assigned 100%. Data are shown as mean ± SD with $n = 3$. *$P < 0.05$, **$P < 0.01$.

the reported ability of Roquin^{M199R} to repress, albeit less efficiently than Roquin^{WT}, huICOS expression [1], indicating that only absence of the ROQ domain can completely abolish the suppressive effects of Roquin on target mRNA.

To test whether presence of the ROQ domain is also essential for Roquin's regulation of endogenous *Icos* mRNA decay, EL4 cells were transfected with Roquin^{WT}, Roquin^{M199R}, Roquin$^{\Delta ROQ}$ or empty vector, rested for 24 h and then stimulated for 6 h with 4β-phorbol 12-myristate 13-acetate and ionomycin. Actinomycin D was added to inhibit transcription and the rate of *Icos* mRNA decay was measured at 30 min intervals over 3 h. Consistent with our previous reports, Roquin^{WT} shortened the half-life of endogenous *Icos* mRNA by ~ 50%, from 94 min (empty vector control) to 43 min (Fig. 5C). This Roquin-dependent reduction in *Icos* mRNA half-life was

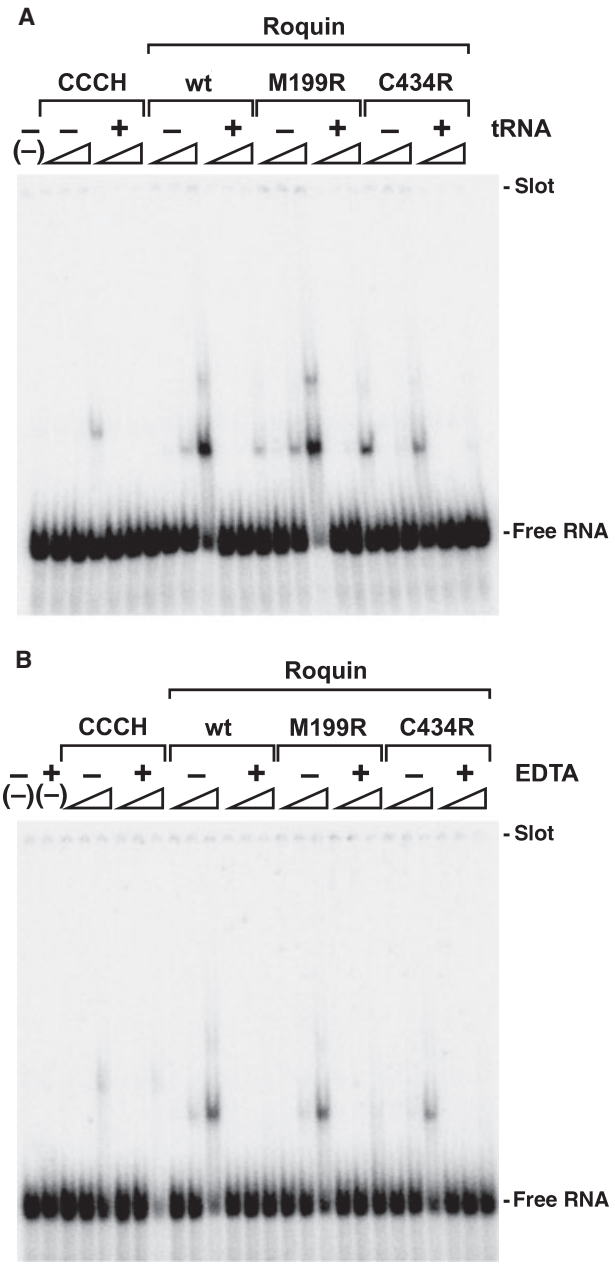

Fig. 6. Roquin binds to a sequence in the *Icos* mRNA 3′-UTR. Recombinant protein fragments corresponding to Roquin amino acids 1–484 [47], or Roquin amino acids 1–484 with the mutations M199R (M199R), C434R (C434R) or Roquin 407–484 (CCCH) were purified and their ability to bind a 47-bp sequence derived from *Icos* mRNA [1] was evaluated in REMSA. (A) Binding after preincubation of recombinant protein fragments in binding buffer containing 5 μM $ZnCl_2$ is indicated by (–) above the relevant lanes. Binding after preincubation in binding buffer containing 5 μM $ZnCl_2$ but also in the presence of 1 μg yeast tRNA as competitor is indicated by (+) above the relevant lanes. (B) Binding after preincubation of recombinant protein fragments in binding buffer containing 5 μM $ZnCl_2$ is indicated by (–) above the relevant lanes. Binding after preincubation of recombinant protein fragments in binding buffer containing 0.5 mM EDTA instead of $ZnCl_2$ is indicated by (+) above the relevant lanes. In all cases, RNA is present at a concentration of 1×10^{-8} M, and where added, proteins are present at a concentration of 1×10^{-8}, 1×10^{-7} or 1×10^{-6} M, calculated per Roquin monomer. Increasing concentration of each added protein is indicated by a wedge above the relevant lanes, and the absence of any added protein is indicated by (–). The position of the free RNA and of the loading slots is indicated to the right of each gel.

abolished by the M199R mutation (92 min), whereas $Roquin^{\Delta ROQ}$ significantly delayed *Icos* mRNA decay, increasing its half-life by over twofold (to 243 min). This suggests that $Roquin^{\Delta ROQ}$ is dominant negative over $Roquin^{WT}$, at least in EL4 cells. Taken together, these results show that the ROQ domain is essential for Roquin's repression of *Icos* mRNA.

Roquin binds *Icos* mRNA

To determine whether Roquin directly binds the portion of the *Icos* 3′-UTR known to be essential for its regulation [1], we overexpressed and purified recombinant protein fragments corresponding to the N-terminal fragment amino acids 1–484 (Fig. 6; Roq1–484) of either wild-type sequence or with the M199R or C434R substitutions, as well as a recombinant protein fragment corresponding to the CCCH domain (amino acids 407–484; Roq407–484). Examination of the binding activity of these recombinant protein fragments to the minimal 47 bp *Icos* mRNA target [1] in RNA electrophoresis mobility shift assay (REMSA) showed that Roquin bound specifically within this region, because the mobility of RNA probes containing the 47 bp target was retarded in the presence of Roquin1–484 (Fig. 6A,B), but the mobility of control RNA probes was not (Fig. S4). Specificity was unaltered by competitor RNA [Fig. 6A; lanes containing addition of non-specific competitor tRNA is indicated by (+)]. The M199R substitution did not affect RNA binding or specificity in these assays (Figs 6 and S4), suggesting that the mutation, predicted to affect local helical structure, may instead impair interaction with a protein-binding partner. The C434R substitution – the third coordinating cysteine in the CCCH zinc finger – reduced but did not completely abolish binding (Fig. 6A), an unexpected result given that a comparable mutation in the zinc-finger-containing RNA-binding protein TTP (C124R) completely abolishes RNA-binding activity [31]. Again, specificity remained unaltered by the substitution (Fig. S4). By contrast, binding activity exhibited by the CCCH domain in isolation was significantly less, with a retarded complex running

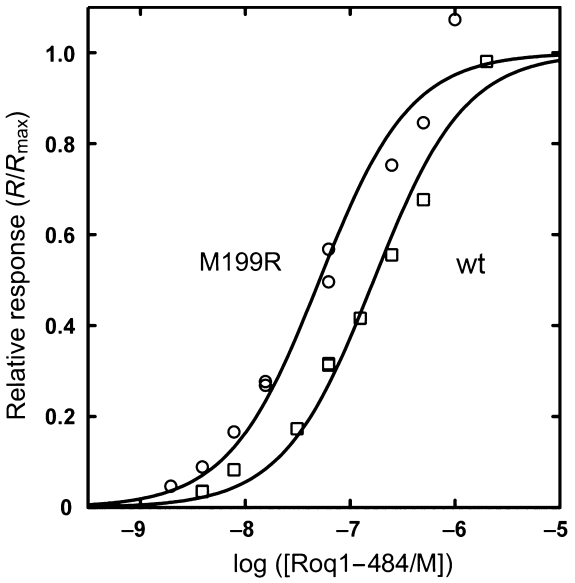

Fig. 7. Roquin binds to the *Icos* mRNA 3′-UTR. Binding isotherms for interaction of Roq1–484 wild-type and M199R with immobilized *Icos* RNA at 20 °C in 10 mM Tris pH 7.4, 150 mM NaCl, as determined by SPR. Raw sensorgrams are shown in Fig. S5. Equilibrium responses (R) at various [protein] were normalized to the saturating response (R_{max}), as determined by fitting to a 1 : 1 Langmuir binding isotherm. Actual R_{max} values were 236 ± 12 RU (for wild-type) and 175 ± 9 RU (M199R). The solid curves were calculated from the derived K_D values of 51 ± 10 nM (for M199R) and 168 ± 25 nM (wild-type).

at a higher molecular mass compared with the larger 1–484 recombinant proteins (Fig. 6) and no complex observable with control RNA (Fig. S4). RNA-binding activity was partly sensitive to challenge with competitor tRNA, which caused reduced binding of wild-type, M199R and C434R Roq1–484 to *Icos* target RNA, and completely blocked binding by Roq407–484 (CCCH domain) [Fig. 6A, lanes with (+) tRNA]. Binding was also sensitive to preincubation of all recombinant protein fragments with EDTA instead of $ZnCl_2$, with EDTA-chelation of Zn^{2+} abolishing all binding [Fig. 6B, addition of EDTA indicated by (+) above relevant lanes]. Neither tRNA nor EDTA treatment induced binding to control target RNA by any of the recombinant protein fragments (data not shown).

Binding of Roquin to the minimal *Icos* mRNA region was also studied in real time using SPR (Biacore T100). Binding of both wild-type and M199R Roq1–484 to a 5′-biotinylated *Icos* 3′-UTR was measured at 20 °C in buffer containing 150 mM KCl. Although degradation of RNA during the experiments prevented the direct measurement of kinetic rate constants, the steady-state affinities between *Icos* RNA and Roquin proteins were determined, as shown in Figs 7 and S6. Both the wild-type and M199R proteins bound *Icos* RNA with high affinity, with M199R binding with almost threefold higher affinity than the wild-type, K_D = 51 ± 10. cf. 168 ± 25 nM.

To determine the minimal Roquin binding site, we conducted RNase footprinting experiments using the same *Icos* mRNA region as a probe and Roq1–484 wild-type, M199R or C434R recombinant protein fragments (Fig. 8). Protection from RNase cleavage indicates a primary binding site. With increasing protein concentration, the region spanning bases 49–60 was the first to show protection from cleavage by the single-strand-specific RNase1 (numbering within the probe sequence is shown in Fig. 8A,B). Within this region, bases U54 and U59 – the two residues most notably cleaved by RNaseA (which preferentially cleaves the 3′-end of single-stranded pyrimidine residues), T_1 (which preferentially cleaves the 3′-end of single-stranded guanine residues) and V_1 (which preferentially cleaves double-stranded RNA regions) – showed significant protection from cleavage with increasing protein concentration.

Within stem-loop 1 (SL1) of the predicted secondary structure (Fig. 8B), G62 was protected from $RNaseT_1$ and $RNaseV_1$ cleavage, whereas G66 and G68 were protected from $RNaseT_1$ but not $RNaseV_1$ cleavage. Given that RNase1 cleaves preferentially after single-stranded bases, the sensitivity of unbound *Icos* RNA to RNase1 between bases 54 and 60 was not anticipated by secondary structure predictions (Fig. 8B), although the preponderance of A–U or G–U base pairs within the proximal portion of the left arm of SL1 predicted for bases 54–80 could lead to a relatively destabilized region and thus greater access for the nuclease compared with the distal portion of this SL which contains more G–C base pairs. Contrary to the left arm of the predicted SL1 structure, few bases within the right arm showed significant nuclease sensitivity. G76 showed sensitivity to $RNaseV_1$ that was protected by increasing Roquin concentration, but cleavage of G76, G77, G80 or G82 by $RNaseT_1$ was not significantly inhibited by increasing protein concentration. Further 3′, G82, which is predicted to be unpaired, unexpectedly showed significant cleavage by the double-strand-specific $RNaseV_1$, and was also protected by increasing protein concentration. It is possible that this base is pairing with C52, the last base in the *Bam*HI cloning site of the vector (assuming that a non-Watson–Crick base pair between U53 and U81 also occurs). In addition, bases A78 to U81 showed RNase1 sensitivity that was protected from cleavage at the highest Roquin concentration examined.

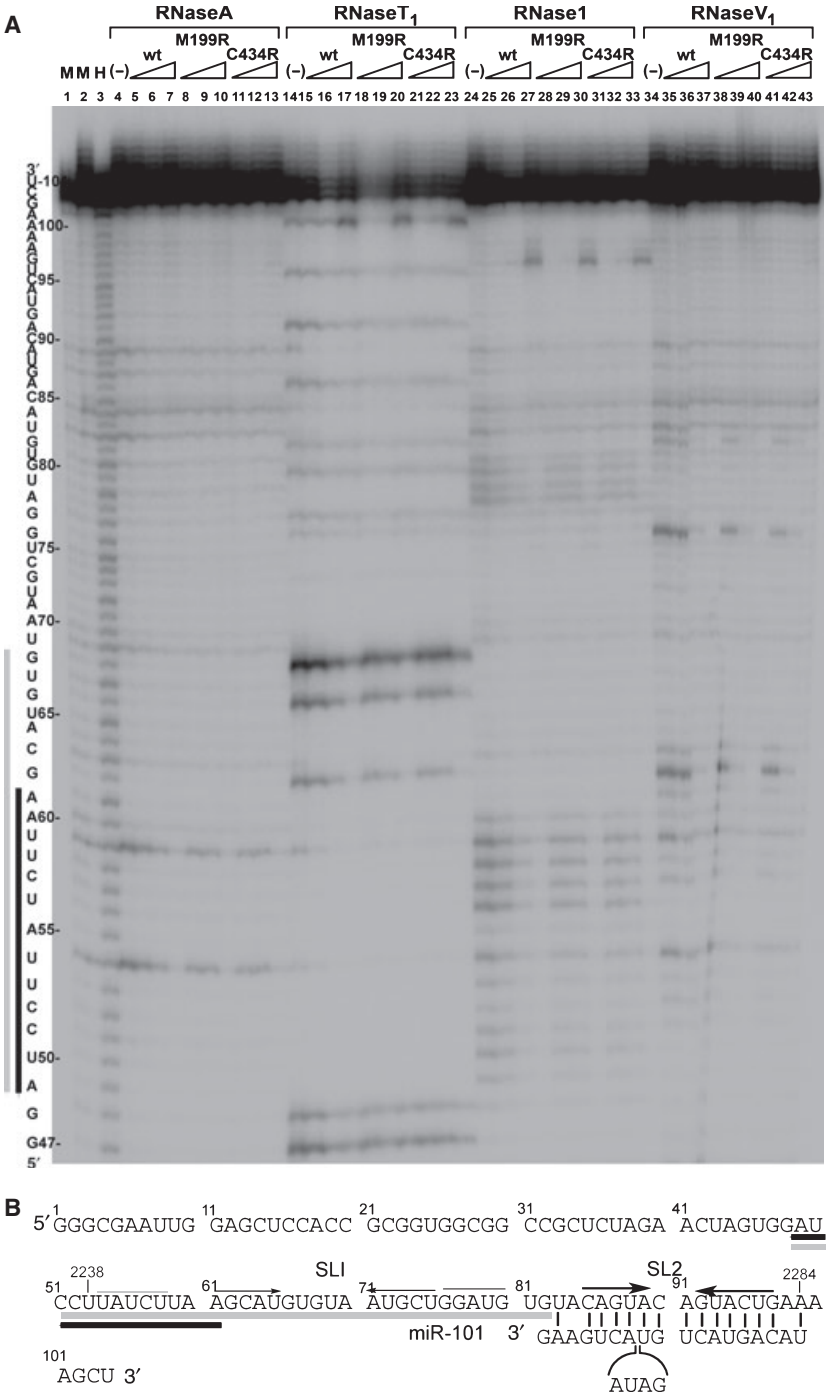

Bases distal to G82 did not show significant protection from any nuclease at the Roquin concentrations examined. In fact, A98 (and to a lesser extent A99 and A100) showed significant hypersensitivity to RNase1 with increasing protein concentration, whereas G102 showed significant hypersensitivity to $RNaseT_1$ with increasing protein concentration. These hypersensitivities could be caused by either changes in RNA secondary structure induced by binding of Roquin, or increased cleavage because of the occupation of more favourable sites by Roquin. Binding by the CCCH domain (Roq407–484) was not examined in these experiments, because the minimal binding observed in the REMSAs (Fig. 6A) suggested that it was unlikely

Fig. 8. Roquin binds to a sequence adjacent to the miR-101 target in the *Icos* mRNA 3′-UTR. A typical RNase footprint analysis of Roq1–484, Roq1–484M199R or Roq1–484C434R binding to *ICOS* RNA is shown. Numbering above the gel indicates the lanes. Lanes 1 and 2 contain two different 'untreated' *Icos* RNA preps and are labeled 'M' (mock). Lane 3 contains *Icos* RNA subjected to partial alkaline hydrolysis in order to generate a ladder of consecutive bases and is labeled 'H'. Lanes 4–13 contain *Icos* RNA partially digested with RNaseA (which cleaves after single stranded Us or Cs) and binding reactions contain: lane 4, no protein; lane 5, 1×10^{-8} M Roquin wild-type; lane 6, 1×10^{-7} M wild-type; lane 7, 1×10^{-6} M wild-type; lane 8, 1×10^{-8} M M199R; lane 9, 1×10^{-7} M M199R; lane 10, 1×10^{-6} M M199R; lane 11, 1×10^{-8} M C434R; lane 12, 1×10^{-7} M C434R; or lane 13, 1×10^{-6} M C434R. The absence of protein is indicated by (–) above the lane, while increasing concentrations of Roquin wild-type, M199R or C434R are indicated by appropriately labeled wedges above the lanes. RNaseA digestion is also indicated by a label above lanes 4–13. Lanes 14–23 are the same as lanes 4–13 except that partial digestion is with $RNaseT_1$ (which cleaves after single stranded Gs). Lanes 24–33 are the same as lanes 4–13 except that partial digestion is with RNase1 (which cleaves preferentially after single stranded residues). Lanes 34–43 are the same as lanes 4–13 except that partial digestion is with $RNaseV_1$ (which cleaves preferentially after base paired residues); labelling is altered to indicate this. On the left side of the gel, bands in the *Icos* mRNA probe ladder are aligned to the *Icos* target RNA. (B) Nucleotide sequence of *Icos*-specific RNA used in the REMSA (Fig. 6) and RNase footprinting experiments. The position of the *Icos*-specific sequence (bases 2238–2284; human *ICOS* accession number NM_012092) is indicated by numbers above the text. A black line under the text indicates the region protected from RNase digestion by the lowest concentration of Roquin1–484, whereas a grey line under the text indicates the region protected from RNase digestion by the highest concentration of Roq1–484 in Fig. 8A. The position of complementarity to miR-101 is also indicated below the text. The most favourable predicted secondary structure for the *Icos* specific RNA (mFold, free energy $\Delta G = -22.63$ kcal·mol^{-1} [46]). The two stem loops within the *ICOS* mRNA sequence referred to in the text are indicated by lines and arrows above the sequence and the letters SL1 or SL2.

that small differences in RNase cleavage would be detected. Significantly, these results show that Roquin is an RNA-binding protein and identify a putative binding sequence within a region of the *Icos* mRNA 3′-UTR previously shown to be essential for *Icos* mRNA degradation by Roquin [1] (Fig. 8B). Interestingly, the Roquin binding sequence is situated immediately upstream of the predicted binding site for miR-101, a microRNA shown to also be critical for *Icos* mRNA degradation [1].

Discussion

Here, we show that the novel immune regulator Roquin is a ubiquitously expressed RNA-binding protein that localizes diffusely and is relocated, along with the markers TIA-1 and eIF3, to cytoplasmic stress granules – sites of mRNA storage in response to stress. Furthermore, Roquin overexpression induces stress granule formation, as reported for other stress granule components including TIA-1 and G3BP. Unlike some RNA-associated proteins such as XRN1, eIF4E, TTP, FAST and RAP55 that shuttle from stress granules to P-bodies [14], which are sites where mRNAs undergo degradation, Roquin appears confined to stress granules. Nevertheless, in cells cotransfected with Roquin and the P-body marker Dcp1a, we noted that a small proportion of cells formed large stress granules in close contact with numerous P-bodies, suggesting that Roquin may also act to recruit P-bodies in a manner similar to TTP.

Roquin's ability to dominantly induce and localize to stress granules is shared by the MNAB protein encoded by the other member of the mammalian *Rc3h* gene family, *Rc3h2*. Stress granule localization is likely to be critical for the function of these proteins, because it is conserved through evolution: the *D. melanogaster* DmRoquin and *C. elegans* RLE-1 homologues were also found in stress granules. With the exception of RLE-1, which lacks a CCCH motif, these proteins are highly conserved in their N-terminal sequences, containing the ROQ domain flanked by a RING and CCCH finger motif. Although it has also been reported that MNAB localizes to the endosomal compartment [28], we were unable to reproduce this finding. This discrepancy may be explained by the use of a different cell type in our experiments.

The absence of Roquin from endosomal compartments suggests that it may not share the endosomal sorting functions of other RING-1 finger domain-containing E3 ubiquitin ligases containing RING-1 finger domains, such as Cbl. Nevertheless, it is possible that the localization of Roquin in HEK 293T used in this study differs from that of other cell types including T cells. Recently the RING-1 finger of the RLE-1 protein was shown to ubiquitinylate DAF-16, a cytoplasmic-nuclear shuttling FOXO transcription factor [22], leading to its degradation by the 26*S* proteosome. The role of the RING-1 zinc finger of Roquin is currently unknown. Polyubiquitylation and proteasome activity have been shown to be required for rapid degradation of mRNAs containing destabilizing ARE elements in their 3′-UTRs, e.g. that of GM-CSF [32]. It is therefore possible that Roquin may induce ubiquitin-mediated degradation of proteins that regulate mRNA stability, or ubiquitin-tagging may alter the localization or association of mRNA regulating proteins.

By creating an extensive series of GFP fusions with the various motifs of Roquin, and by selectively deleting domains from the full-length protein, we determined that the ROQ domain in the N-terminus of the protein is the minimal region required for stress granule induction and localization. It is striking that this domain is the most highly conserved part of the Roquin family of proteins, with ~ 87% identity and ~ 96% similarity in the stress granule-active segment between amino acids 138 and 337 of mammalian and *Drosophila* Roquin homologues (see Fig. S11 in Vinuesa *et al*. [2]). By contrast, the RING-1 and CCCH domains are less well conserved. How does this domain recruit Roquin to stress granules? RNA-binding proteins such as TIA-1, FMRP1 and G3BP contain aggregation/multimerization domains that have been shown to be actively required for stress granule formation [6,8,33,34]. In the case of FMRP1, G3BP and the TTP homologue zinc-finger protein 36 (TIS11), the RNA-binding motif(s) is required to recruit the respective proteins to stress granules [6,8,34,35]. Thus, deletion of either the RNA recognition motif RNA-binding domain or the protein–protein interaction domain of FMRP abolished localization of FMRP and its interacting partners, the fragile-X-related proteins FXR1P and FXR2P, to stress granules [8,34]. The neuronal ELAV-like proteins HuB, HuC and HuD are another family of RNA-binding proteins that stabilize mRNAs and have been shown to form homo- and heterocomplexes with each other [36]. Yeast two-hybrid assays (data not shown) indicated that the ROQ domain does not self-oligomerize, but it is still possible that Roquin may form multimeric complexes either upon RNA binding, potentially including the related MNAB protein that also contains a ROQ domain or other binding partner, and this interaction may recruit Roquin to stress granules.

Roquin decreases the stability of target mRNAs, such as that of *Icos*, by acting on their 3′-UTR, and this is critical to prevent lupus-associated symptoms. The M199R mutation in the ROQ domain impairs this function of Roquin. We have also shown that an intact ROQ domain is essential for the ability of Roquin to regulate the stability of this target mRNA. A recent report has shown that the stress granule translation inhibition machinery is active during T-helper cell differentiation [11], and our results reveal that absence of the ROQ domain prevents Roquin from localizing to stress granules. It is likely that localization to this compartment is important for Roquin's function.

The presence of a single CCCH motif is rare in CCCH family members and it has been shown that tandem CCCH motifs are required for TTP to bind RNA [37,38], and for rat TIS11 to localize to stress granules [35]. In fact, many RNA-binding proteins contain multiple RNA-binding motifs (K-homology domains or RNA recognition motifs) in order to form specific and stable RNA interactions [39]. Roquin1–484 encompassing the ROQ domain exhibits specific RNA-binding activity, but the minimal CCCH recombinant protein fragment (Roquin407–484) shows at best residual activity. This may be explained, at least in part, by examining the nuclear magnetic resonance structure of the CCCH-containing TIS11d bound to RNA, where a critical interaction involves a side chain (Y170) intercalating between adjacent uracils in the bound RNA [40]. Substitution of Y170 by an arginine completely abolishes RNA binding by TIS11d, in spite of the presence of a second intact CCCH domain [31,40]. In the case of Roquin, the comparable residue is an arginine (R430). In addition, the M199R mutation within the ROQ domain, which modestly strengthens rather than impairing RNA-binding activity (Fig. 7), and the C434R mutation which does not completely abolish binding (Fig. 6), strongly suggests that residues outside of the minimal CCCH and most likely within the ROQ domain contribute to specific RNA binding. This may also explain why Roquin's CCCH zinc-finger domain fused to GFP did not localize to stress granules even in arsenite-treated cells. The complex of RNA bound to the minimal CCCH domain also appeared to run at a higher mobility than the 1–484 protein–RNA complexes (Fig. 6). One possible explanation for this is that the CCCH protein may bind RNA as a dimer, analogous to TTP/TIS11, each of which contains two CCCH domains in tandem, whereas the 1–484 proteins may initially bind as monomers and then dimerize, thus contributing to the high and low molecular mass complexes seen in the REMSA gels (Fig. 6). The minimal ROQ domain does not contain obvious features that would indicate it is able to directly bind RNA; it is not predicted to be highly basic overall. It may act to stabilize the interaction between the CCCH zinc-finger domain and target RNA(s) by creating extra contacts with RNA. It is likely that substitution of arginine for methionine caused by the M199R mutation, enhances RNA binding by increasing the basic nature of the domain. The precise role of the ROQ domain, and/or the CCCH motif, in contributing to RNA binding remains to be determined in future detailed structural and mutagenic studies.

Roquin represses *Icos* mRNA through the microRNA machinery. MicroRNAs are small noncoding RNAs known to regulate translation and/or stability of target gene mRNAs in P-bodies. *Icos* mRNA was found to localize to both stress granules and P-bodies [1], whereas Roquin itself does not appear to be in the latter compartment. We have observed close associa-

tion of most P-bodies with stress granules in cells where Roquin is overexpressed. This suggests that Roquin might mediate recruitment of P-bodies into close contact with stress granules. The regulatory activity of miRNAs has been shown to be dependent on their localization in stress granules or P-bodies [41]. Because the sites within the *Icos* 3′-UTR contacted by Roquin and miR-101 are adjacent, it is possible that Roquin binding facilitates miR-101 access through binding-induced changes in RNA secondary structure. Previous studies have shown that RNA-binding proteins binding adjacent to miRNA-binding sites in target mRNAs can affect repression [42,43]. Whether the juxtaposition of stress granules and P-bodies is a consequence of the adjacent binding sites or Roquin is also interacting directly with miR-101 or other P-body components, remains to be determined.

The consequences of the Roquin mutation in *sanroque* mice are failure to repress target mRNAs such as *Icos* and the development of a devastating autoimmune disease. Our studies have revealed that this mutation does not impair Roquin's ability to bind mRNA, but instead appears to strengthen this binding. Stronger binding could be detrimental to Roquin's ability to repress target RNAs, i.e. by preventing their transfer to P-bodies. Alternatively, it is possible the mutation impairs binding to a key protein or changes the overall structure of the ROQ domain, impairing concomitant binding of Roquin and miRNA to the target mRNA. Elucidating how Roquin regulates the metabolism of target mRNAs in stress granules may therefore have important implications for our understanding of adaptive immune responses and the pathogenesis of autoimmunity.

Materials and methods

Cell lines and transfection

HEK 293T cells were obtained from the American Type Culture Collection and were maintained in Dulbecco's modified Eagle's medium containing 10% fetal bovine serum at 5% CO_2. Semiconfluent cells were transfected in six-well plates with 3 μg total plasmid DNA using the calcium phosphate transfection protocol. Transfection media was removed 14–24 h later, and cells were moved to coverslips and allowed to adhere overnight before processing for microscopy. To aid adherence, Jurkat cells were transferred to concanavalin A (50 $\mu g \cdot mL^{-1}$)-treated coverslips and allowed to settle for 1 h. Jurkat and EL4 cells were grown in RPMI medium supplemented with 10% fetal bovine serum and antibiotics. EL4 cells were transfected using lipofectamine 2000 (Invitrogen, Carlsbad, CA, USA).

Retroviral transductions

The construction of various *huICOS* fragments, packaging of retroviruses and transduction of NIH3T3 cells and primary $CD4^+$ T cells have been described previously [1]. In brief, retroviral supernatants were harvested from packaging Phoenix cells transfected with individual retroviral constructs. NIH3T3 cells and primary $CD4^+$ T cells were transduced by retroviruses using spinoculation. Flow cytometry was performed as described previously [2].

Antibodies

Antibodies against TIA-1 and eIF3η were obtained from Santa Cruz Biotechnology (Santa Cruz, CA, USA), antibody against Dcp1 was obtained from Abcam (Abcam Inc., Cambridge, MA, USA) and antibody against human Roquin (NB100-655) was purchased from Novus Biologicals (Novus Biologicals LLC, Littleton, CO, USA). Antibodies were used at 1 : 75 in immunofluorescence studies. Secondary antibodies conjugated to Alexa 568 or Alexa 488 were purchased from Molecular Probes (Invitrogen).

Plasmids

To make Roquin–GFP, the mouse Roquin gene was amplified from C57BL/6 mouse spleen cDNA as described previously [2]. All mutations in the Roquin domains were introduced by site-directed mutagenesis (Stratagene, La Jolla, CA, USA). Truncation variants of Roquin were all constructed by PCR amplification of the specified regions and cloned into pCDNA3.1 CT–GFP TOPO TA fusion vector (Invitrogen) or pGEX-6P-3 (Amersham, GE Healthcare Biosciences, Piscataway, NJ, USA) for overexpression. The coding sequences of human MNAB, TIA-1 and Dcp1a were PCR amplified from HEK 293 T cDNA and cloned into the vectors pCDNA3.1 CT–GFP TOPO TA and DsRed express N1, which encodes a more soluble version of DsRed (Clontech Laboratories Inc., Mountain View, CA, USA). The cDNA of *DmRoquin* was obtained from the Berkeley *Drosophila* Gene Collection and that of RLE-1 from Y. Kohara (National Institute of Genetics, Mishima, Japan). The mouse GFP–Hrs construct was a gift from P. Davey (University of Adelaide, Australia) and was used to subclone the *hrs* gene into DsRedexpress N1. A 50bp region from *Icos* mRNA was PCR amplified and cloned into pBSII KS (+) for *in vitro* transcription of the probe used in REMSA and RNA footprinting experiments.

Fluorescence microscopy

Cells transfected with fluorescently tagged constructs were fixed in 3.7% formaldehyde, permeabilized with 1% Triton X-100 for 5 min, washed in NaCl/P_i and counter-

stained with 4′,6-diamidino-2-phenylindole for 5 min before mounting in Vectashield. Antibody staining with TIA-1 was as described previously with some modifications [2]. Cells were fixed for 10 min in 3% paraformaldehyde, permeabilized in 0.5% Triton X-100, washed in NaCl/P_i and blocked in 5% fetal bovine serum/5% BSA for 1 h at room temperature. TIA-1 was used at 1 : 75 and Alexa 568 at 1 : 375. Cells were viewed on a Deltavision system (Applied Precision Inc., Issaquah, WA, USA) mounted on an Olympus IX70 inverted microscope using an Olympus 60 × oil objective PlanApo (NA 1.40). Images were collected with a Photometrics CH350 CCD camera using SOFTWORX acquisition software (Applied Precision). Deconvolution was performed with SOFTWORX, average intensity projections representing 0.5-mm sections taken and final images compiled using Adobe PHOTOSHOP. For imaging the cellular localization of individual constructs, images were projections from 10 Z sections of 0.5 mm per section, whereas single Z sections of 0.5 mm thickness were used in colocalization studies.

Real time RT-PCR

EL4 cells transfected with empty pCDNA3.1GFP vector, $Roquin^{WT}$, $Roquin^{M199R}$ or $Roquin^{\Delta ROQ}$ domain mutant constructs were rested for 24 h and then stimulated with 50 ng·mL^{-1} 4β-phorbol 12-myristate 13-acetate and 0.5 mg·mL^{-1} ionomycin for 6 h. After 6 h, actinomycin D (10 μg·mL^{-1}) was added to block *de novo* transcription, and total RNA was isolated after 0, 30, 60, 120 and 180 min using TRIzol and treated with DNase I (Invitrogen) to avoid DNA contamination. SuperScript III Reverse Transcriptase (Invitrogen) was then used to prepare cDNA with $oligo(dT)_{12–18}$ as primer. *Icos* mRNA levels were measured using real-time PCR and normalized to those of β-actin. Primer sequences are available on request. The normalized level of *Icos* mRNA at time 0 was set at 100%, and all other normalized mRNA levels were plotted relative to that value. Each point on the graph is represented by the mean ± SEM of duplicate samples and representative of three independent experiments.

Recombinant protein overexpression and purification

Constructs spanning amino acids 1–484, 1–484 containing the M199R mutation and the CCCH zinc finger (407–484) of the mouse Roquin protein were overexpressed as glutathione *S*-transferase fusions in *Escherichia coli* Rosetta (gami DE3) pLysS (Novagen) in the presence of 150 μM $ZnSO_4$ in the growth media, and purified using glutathione *S*-transferase resin (Amersham, GE Healthcare) with the addition of 5 μM $ZnCl_2$ in all purification buffers. The Roquin recombinant protein fragments were cleaved with PreScission protease (Amersham) and concentrated using Amicon Ultra-4 centrifugal filters (Millipore, Billerica, MA, USA). Gel filtration of proteins was carried out on a HiPrep 16/60 Sephacryl S-300 high-resolution column (Amersham) and concentrated again for use in RNA-binding studies.

RNA-binding assays

Target RNAs were generated by linearizing either control (empty vector) or *Icos* minimal region-containing pBluescriptII KS [pBSII KS (+)] (Stratagene) with *Hin*dIII then transcribing with T7 RNA polymerase *in vitro* (Ambion MEGA Shortscript, Applied Biosystems/Ambion Inc., Austin, TX, USA). After gel purification of full-length transcripts, target RNAs were end-labelled with [^{32}P]ATP[γP] using T4 polynucleotide kinase (Ambion) and then subjected to a second round of gel purification prior to use. Purified proteins were diluted to 2 × final concentration in 1 × binding buffer (10 mM Tris/HCl pH 7.5, 40 mM KCl, 5 μM $ZnCl_2$ or 0.5 mM EDTA as indicated, 1 mM dithiothreitol, 50 μg·mL^{-1} w/v BSA, 5% v/v glycerol) and allowed to equilibrate for 20 min at room temperature prior to use [44]. Target RNAs (in H_2O) were diluted to 4 × final concentration (in H_2O), heated for 10 min at 75 °C then quenched on ice prior to the addition of an equal volume of 2 × binding buffer immediately prior to use. Diluted protein and RNA were then mixed (final volume = 10 μL) and incubated at room temperature for 30 min. Where added, competitor tRNA (1 μL of a 1 μg·μL^{-1} solution) was mixed with 5 μL of 2 × final concentration of protein and incubated for 10 min at room temperature prior to mixing with probe RNA. After incubation, 4 μL loading buffer (1 × binding buffer containing 50% v/v glycerol and 0.04% w/v each bromophenol blue and xylene cyanol) was added and the mixture immediately loaded onto nondenaturing PAGE gels for electrophoresis [45].

RNase footprinting reactions

For RNase footprint reactions, protein and RNA were treated as described for RNA-binding assays and binding reactions were performed in a total volume of 60 μL. After the 30-min incubation, 10 μL of the mixture was removed for REMSA as above. RNase footprint reactions were then performed by removing 10 μL aliquots of the binding reaction and mixing with 1 μL of each of RNaseA, $RNaseT_1$, RNase1 or $RNaseV_1$ (Ambion; the cited cleavage specificities are according to manufacturers specifications), diluted in H_2O to a concentration predetermined in pilot experiments to give an appropriate digestion pattern, and incubated for 15 min at room temperature. Proteinase K and SDS were then added to a final concentration of 0.25 μg and 0.05% (w/v), respectively, in a total volume of 100 μL and the mixture was incubated for a further 15 min at room temperature, prior to extraction once with phenol/chloroform/iso-amyl alcohol (25: 24: 1 v/v/v) and precipitation of RNA from the aqueous phase. Pellets were resuspended in 7 μL formamide/dye

(95% formamide, 18 mM EDTA, 0.025% w/v SDS, 0.025% w/v bromophenol blue, 0.025% w/v xylene cyanol) prior to electrophoresis of half on sequence gels. 'Untreated' negative control RNAs were incubated with 1 μL H_2O rather than any RNase, but were otherwise handled in an identical manner. RNA ladders were generated by incubating 5′ end-labelled RNA with 0.1 μg yeast tRNA in a total volume of 5 μL of 50 mM Na_2CO_3 pH 9.2, 1 mM EDTA at 95 °C for 5 min, then quenching on ice. Ten microlitres of formamide/dye (as above) were added to the mixture prior to electrophoresis of 5 μL of the total. After electrophoresis, for both REMSA and RNase footprint experiments, gels were transferred to Whatman 3M filter paper, dried and exposed to phosphorimager plates for band detection. RNA secondary structure predictions were performed using the web-based Mfold algorithm [46].

SPR measurements

For SPR, Roquin 1–484 wild-type and M199R were freshly dialysed into SPR buffer [10 mM Tris pH 7.4, 150 mM NaCl, 1 mM tris(2-carboxyethyl)phosphine, 0.05% surfactant P-20]. Measurements were made at 20 °C on a Biacore T100 SPR instrument (GE Healthcare) at a flow rate of 50 $\mu L \cdot min^{-1}$. 5′-Biotinylated *Icos* 3′-UTR RNA corresponding to: GGAUCCUUAUCUUAAGCAUGUGUAAUGC UGGAUGUGUACAGUAC (Shanghai GenePharma Co. Ltd, Shanghai, China) was dissolved in water to 20 μM, then diluted to 1 μM in SPR buffer, heated to 80 °C for 5 min and allowed to slowly cool (∼ 15 min). It was further diluted to 20 nM before immobilization of 200 response units (RU) onto a single flow cell of a streptavidin-coated Biacore (SA) chip by injection at 10 $\mu L \cdot min^{-1}$ for ∼ 100 s. A second flow cell was left underivatized for blank subtraction. Surfaces were regenerated by injection of 1 M $MgCl_2$ for 1 min at 5 $\mu L \cdot min^{-1}$, leaving the RNA intact but removing bound protein. Association was measured for 180 s and Roquin was allowed to dissociate for 300 s before regeneration. Roq1–484 wild-type was used in twofold serial dilutions from 2000 to 7.8 nM, and M199R was from 1000 to 3.9 nM, with injections for each protein being in random order. Simple first-order rate constants could not be derived from the association and dissociation kinetics (Fig. S5), so steady-state binding responses were used to approximate affinity K_D values. Although experiments were repeated twice, progressive degradation of the immobilized RNA prevented use of replicates in data fitting. A dataset comprising the first 10 cycles measured for each protein was selected to minimize effects from chip degradation (see Fig. S5).

Acknowledgements

This work was funded by a Viertel Senior Medical Research Fellowship to CGV, an NH&MRC program grant to CGV and CCG, and the ARC Special Research Centre for the Molecular Genetics of Development (CMGD). We acknowledge K. Hill for help in making some of the constructs.

References

1 Yu D, Tan H-MA, Hu X, Athanasopoulos V, Simpson N, Silva DG, Hutloff A, Giles KM, Leedman PJ, Lam KP *et al.* (2007) Roquin represses autoimmunity by limiting inducible T-cell co-stimulator messenger RNA. *Nature* **450**, 299–304.

2 Vinuesa CG, Cook MC, Angelucci C, Athanasopoulos V, Rui L, Hill KM, Yu D, Domaschenz H, Whittle B, Lambe T *et al.* (2005) A RING-type ubiquitin ligase family member required to repress follicular helper T cells and autoimmunity. *Nature* **435**, 452–458.

3 McInerney GM, Kedersha NL, Kaufman RJ, Anderson P & Liljestrom P (2005) Importance of eIF2alpha phosphorylation and stress granule assembly in alphavirus translation regulation. *Mol Biol Cell* **16**, 3753–3763.

4 Bond U (2006) Stressed out! Effects of environmental stress on mRNA metabolism. *FEMS Yeast Res* **6**, 160–170.

5 Kedersha NL, Gupta M, Li W, Miller I & Anderson P (1999) RNA-binding proteins TIA-1 and TIAR link the phosphorylation of eIF-2 alpha to the assembly of mammalian stress granules. *J Cell Biol* **147**, 1431–1442.

6 Tourriere H, Chebli K, Zekri L, Courselaud B, Blanchard JM, Bertrand E & Tazi J (2005) The RasGAP-associated endoribonuclease G3BP assembles stress granules. *J Cell Biol* **160**, 823–831.

7 Kedersha N, Chen S, Gilks N, Li W, Miller IJ, Stahl J & Anderson P (2002) Evidence that ternary complex (eIF2-GTP-tRNA(i)(Met))-deficient preinitiation complexes are core constituents of mammalian stress granules. *Mol Biol Cell* **13**, 195–210.

8 Mazroui R, Huot ME, Tremblay S, Filion C, Labelle Y & Khandjian EW (2002) Trapping of messenger RNA by Fragile X Mental Retardation protein into cytoplasmic granules induces translation repression. *Hum Mol Genet* **11**, 3007–3017.

9 Anderson P & Kedersha N (2006) RNA granules. *J Cell Biol* **172**, 803–808.

10 Kim WJ, Back SH, Kim V, Ryu I & Jang SK (2005) Sequestration of TRAF2 into stress granules interrupts tumor necrosis factor signaling under stress conditions. *Mol Cell Biol* **25**, 2450–2462.

11 Scheu S, Stetson DB, Reinhardt RL, Leber JH, Mohrs M & Locksley RM (2006) Activation of the integrated stress response during T helper cell differentiation. *Nat Immunol* **7**, 644–651.

12 Sheth U & Parker R (2003) Decapping and decay of messenger RNA occur in cytoplasmic processing bodies. *Science* **300**, 805–808.
13 Cougot N, Babajko S & Seraphin B (2004) Cytoplasmic foci are sites of mRNA decay in human cells. *J Cell Biol* **165**, 31–40.
14 Kedersha N, Stoecklin G, Ayodele M, Yacono P, Lykke-Andersen J, Fitzler MJ, Scheuner D, Kaufman RJ, Golan DE & Anderson P (2005) Stress granules and processing bodies are dynamically linked sites of mRNP remodeling. *J Cell Biol* **169**, 871–884.
15 Liu J, Valencia-Sanchez MA, Hannon GJ & Parker R (2005) MicroRNA-dependent localization of targeted mRNAs to mammalian P-bodies. *Nat Cell Biol* **7**, 719–723.
16 Rehwinkel J, Behm-Ansmant I, Gatfield D & Izaurralde E (2005) A crucial role for GW182 and the DCP1:DCP2 decapping complex in miRNA-mediated gene silencing. *RNA* **11**, 1640–1647.
17 Brengues M, Teixeira D & Parker R (2005) Movement of eukaryotic mRNAs between polysomes and cytoplasmic processing bodies. *Science* **310**, 486–489.
18 Wilczynska A, Aigueperse C, Kress M, Dautry F & Weil D (2005) The translational regulator CPEB1 provides a link between dcp1 bodies and stress granules. *J Cell Sci* **118**, 981–992.
19 Kedersha N & Anderson P (2002) Stress granules: sites of mRNA triage that regulate mRNA stability and translatability. *Biochem Soc Trans* **30**, 963–969.
20 Kopito RR (2000) Aggresomes, inclusion bodies and protein aggregation. *Trends Cell Biol* **10**, 524–530.
21 Garcia-Mata R, Bebok Z, Sorscher EJ & Sztul ES (1999) Characterization and dynamics of aggresome formation by a cytosolic GFP-chimera. *J Cell Biol* **146**, 1239–1254.
22 Li W, Gao B, Lee S-M, Bennett K & Fang D (2007) RLE-1, an E3 ubiquitin ligase, regulates C. elegans aging by catalyzing DAF-16 polyubiquitination. *Dev Cell* **12**, 235–246.
23 Jiang X & Sorkin A (2003) Epidermal growth factor receptor internalization through clathrin-coated pits requires Cbl RING finger and proline-rich domains but not receptor polyubiquitylation. *Traffic* **4**, 529–543.
24 Hicke L & Dunn R (2003) Regulation of membrane protein transport by ubiquitin and ubiquitin-binding proteins. *Annu Rev Cell Dev Biol* **19**, 141–172.
25 Mueller DL (2004) E3 ubiquitin ligases as T cell anergy factors. *Nat Immunol* **5**, 883–890.
26 Kim GH, Park E, Kong YY & Han JK (2006) Novel function of POSH, a JNK scaffold, as an E3 ubiquitin ligase for the Hrs stability on early endosomes. *Cell Signal* **18**, 553–563.
27 Shin ME, Ogburn KD, Varban OA, Gilbert PM & Burd CG (2001) FYVE domain targets Pib1p ubiquitin ligase to endosome and vacuolar membranes. *J Biol Chem* **276**, 41388–41393.
28 Siess DC, Vedder CT & Merkens LS (2000) A human gene coding for a membrane-associated nucleic acid-binding protein. *J Biol Chem* **275**, 33655–33662.
29 Laroia G, Cuesta R, Brewer G & Schneider RJ (1999) Control of mRNA decay by heat shock-ubiquitin-proteasome pathway. *Science* **284**, 499–502.
30 Joazeiro CA, Wing SS, Huang H, Leverson JD, Hunter T & Liu YC (1999) The tyrosine kinase negative regulator c-Cbl as a RING-type, E2-dependent ubiquitin-protein ligase. *Science* **286**, 309–312.
31 Lai WS, Kennington EA & Blackshear PJ (2002) Interactions of CCCH zinc finger proteins with mRNA: non-binding tristetraprolin mutants exert an inhibitory efect on degradation of AU-rich element-containing mRNAs. *J Biol Chem* **277**, 9606–9613.
32 Laroia G, Sarkar B & Schneider RJ (2002) Ubiquitin-dependent mechanism regulates rapid turnover of AU-rich cytokine mRNAs. *Proc Natl Acad Sci U S A* **99**, 1842–1846.
33 Gilks N, Kedersha N, Ayodele M, Shen L, Stoecklin G, Dember LM & Anderson P (2004) Stress granule assembly is mediated by prion-like aggregation of TIA-1. *Mol Biol Cell* **15**, 5383–5398.
34 Mazroui R, Huot ME, Tremblay S, Boilard N, Labelle Y & Khandjian EW (2003) Fragile X Mental Retardation protein determinants required for its association with polyribosomal mRNPs. *Hum Mol Genet* **12**, 3087–3096.
35 Murata T, Morita N, Hikita K, Kiuchi K & Kaneda N (2005) Recruitment of mRNA-destabilizing protein TIS11 to stress granules is mediated by its zinc finger domain. *Exp Cell Res* **303**, 287–299.
36 Kasashima K, Sakashita E, Saito K & Sakamoto H (2002) Complex formation of the neuron-specific ELAV-like Hu RNA-binding proteins. *Nucleic Acids Res* **30**, 4519–4526.
37 Lai WS, Carballo E, Strum JR, Kennington EA, Phillips RS & Blackshear PJ (1999) Evidence that tristetraprolin binds to AU-rich elements and promotes the deadenylation and destabilization of tumor necrosis factor alpha mRNA. *Mol Cell Biol* **19**, 4311–4323.
38 Lai WS, Carballo E, Thorn JM, Kennington EA & Blackshear PJ (2000) Interactions of CCCH zinc finger proteins with mRNA: binding of tristetraprolin-related zinc finger proteins to AU-rich elements and destabilization of mRNA. *J Biol Chem* **275**, 17827–17837.
39 Gibson TJ, Rice PM, Thompson JD & Heringa J (1993) KH domains within the FMR1 sequence suggest that fragile X syndrome stems from a defect in RNA metabolism. *Trends Biochem Sci* **18**, 331–333.
40 Hudson BP, Martinez-Yamout MA, Dyson HJ & Wright PE (2004) Recognition of the mRNA AU-rich

element by the zinc finger domain of TIS11d. *Nat Struct Mol Biol* **11**, 257–264.
41 Leung AKL & Sharp PA (2007) microRNAs: a safeguard against turmoil? *Cell* **130**, 581–585.
42 Bhattacharyya SN, Habermacher R, Martine U, Closs EI & Filipowicz W (2006) Relief of microRNA-mediated translational repression in human cells subjected to stress. *Cell* **125**, 1111–1124.
43 Vasudevan S, Tong Y & Steitz JA (2007) Switching from repression to activation: microRNAs can up-regulate translation. *Science* **318**, 1931–1934.
44 Brewer BY, Malicka J, Blackshear PJ & Wilson GM (2004) RNA sequence elements required for high affinity binding by the zinc finger domain of tristetraprolin: conformational changes coupled to the bipartite nature of AU-rich mRNA-destabilizing motifs. *J Biol Chem* **279**, 27870–27877.
45 Oehler S, Alex R & Barker A (1999) Is nitrocellulose filter binding really a universal assay for protein-DNA interactions? *Anal Biochem* **268**, 330–336.
46 Zuker M (2003) Mfold web server for nucleic acid folding and hybridization prediction. *Nucleic Acids Res* **31**, 3406–3415.
47 Yang D, Chen Q, Rosenberg HF, Rybak SM, Newton DL, Wang ZY, Fu Q, Tchernev VT, Wang M, Schweitzer B *et al*. (2004) Human ribonuclease A superfamily members, eosinophil-derived neurotoxin and pancreatic ribonuclease, induce dendritic cell maturation and activation. *J Immunol* **173**, 6134–6142.

Supporting information

The following supplementary material is available:
Fig. S1. Roquin+ granules are dissolved by cycloheximide and are not aggresomes.
Fig. S2. MNAB, RLE-1 and DmRoquin are recruited to stress granules.
Fig. S3. Effects of different protein domains and mutations on the localization of Roquin and MNAB.
Fig. S4. Roquin binds specifically to a sequence in the *Icos* mRNA 3′-UTR.
Fig. S5. SPR study of binding of Roq1–484 proteins to 5′-biotinylated *Icos* 3′-UTR RNA at 20 °C in neutral buffer containing 150 mM NaCl.

This supplementary material can be found in the online version of this article.

Please note: As a service to our authors and readers, this journal provides supporting information supplied by the authors. Such materials are peer-reviewed and may be re-organized for online delivery, but are not copy-edited or typeset. Technical support issues arising from supporting information (other than missing files) should be addressed to the authors.